GeroScience (2022) 44:349–369
https://doi.org/10.1007/s11357-021-00476-1

ORIGINAL ARTICLE

Aging-induced impaired endothelial wall shear stress mechanosensing causes arterial remodeling via JAM-A/F11R shedding by ADAM17

Yanna Tian · Katie Anne Fopiano · Vadym Buncha · Liwei Lang · R. Daniel Rudic · Jessica A. Filosa · Huijuan Dou · Zsolt Bagi

Received: 20 May 2021 / Accepted: 8 October 2021 / Published online: 30 October 2021

Abstract Physiological and pathological vascular remodeling is uniquely driven by mechanical forces from blood flow in which wall shear stress (WSS) mechanosensing by the vascular endothelium plays a pivotal role. This study aimed to determine the novel role for a disintegrin and metalloproteinase 17 (ADAM17) in impaired WSS mechanosensing, which was hypothesized to contribute to aging-associated abnormal vascular remodeling. Without changes in arterial blood pressure and blood flow rate, skeletal muscle resistance arteries of aged mice (30-month-old vs. 12-week-old) exhibited impaired WSS mechanosensing and displayed inward hypertrophic arterial remodeling. These vascular changes were recapitulated by in vivo confined, AAV9-mediated overexpression of ADAM17 in the resistance arteries of young mice. An aging-related increase in ADAM17 expression reduced the endothelial junction level of its cleavage substrate, junctional adhesion molecule-A/F11 receptor (JAM-A/F11R). In cultured endothelial cells subjected to steady WSS ADAM17 activation or JAM-A/F11R knockdown inhibited WSS mechanosensing. The ADAM17-activation induced, impaired WSS mechanosensing was normalized by overexpression of ADAM17 cleavage resistant, mutated JAM-A^{V232Y} both in cultured endothelial cells and in resistance arteries of aged mice, in vivo. These data demonstrate a novel role for ADAM17 in JAM-A/F11R cleavage-mediated impaired endothelial WSS mechanosensing and subsequently developed abnormal arterial remodeling in aging. ADAM17 could prove to be a key regulator of WSS mechanosensing, whereby it can also play a role in pathological vascular remodeling in diseases.

Keywords Aging · Endothelium dysfunction · Mechano-transduction · F11R · Junctional adhesion molecule-A

Supplementary Information The online version contains supplementary material available at https://doi.org/10.1007/s11357-021-00476-1.

Y. Tian · K. A. Fopiano · V. Buncha · L. Lang · J. A. Filosa · H. Dou · Z. Bagi (✉)
Department of Physiology, Medical College of Georgia, Augusta University, Augusta, GA 30912, USA
e-mail: zbagi@augusta.edu

R. D. Rudic
Department of Pharmacology and Toxicology, Medical College of Georgia, Augusta University, Augusta, GA 30912, USA

H. Dou
Department of Medicine, Columbia University Medical Center, New York, NY 10032, USA

Introduction

In aging, important changes in the cardiovascular system develop, including increased stiffness and abnormal remodeling of blood vessels which can independently predict cardiovascular events and mortality

[18, 23, 36]. While the underlying mechanisms of age-related, large artery remodeling, and vascular stiffening are established [10, 12, 53, 54], the cause of aging-induced remodeling of small resistance arteries remains elusive. Functional and structural changes in the microcirculation of various organs have been previously described in aged rodent models [6, 24]. Studies have shown that aging-associated remodeling of small resistance arteries can occur independently from changes in systemic blood pressure [21, 30, 34, 53, 54]. It has been long recognized that small resistance arteries can undergo remodeling in response to lasting changes in blood flow or blood flow cessation [38]. However, throughout the lifespan, organs receive optimal or even greater than normal blood flow [22], unless significant stenosis or occlusion of larger arteries develops, thus seemingly questioning the mechanistic role of altered blood flow in age-related vascular remodeling. It should be noted that it is not the rate of blood flow but wall shear stress (WSS), the tangential force driven by the friction of the flowing blood on the endothelial cell surface, plays the key role in vascular regulation and signaling [11, 28, 29]. WSS is determined by blood flow velocity, viscosity, and the vascular luminal diameter [11]. In resistance arteries, temporal increases in WSS induces vasodilation whereby WSS contributes to a feedforward regulation of tissue perfusion [11, 28, 29]. Long-term WSS can directly influence vascular wall remodeling and vascular growth in the microcirculation. For example, small collateral arteries remodel and expand in response to increases in WSS, whereas a reduction in WSS causes lumen narrowing arterial remodeling [1, 2, 58]. Interestingly, an early study by Sun et al. has found that reduced flow-induced dilation is mediated by impaired WSS sensitivity in skeletal muscle resistance arteries in 29–32-week-old, mid-aged adult rats [46]. In the present study, we raised the possibility that in aging resistance arteries undergo abnormal lumen narrowing remodeling even without changes in the rate of blood flow owing to the vascular endothelium's inability to properly sense WSS.

Sensing of WSS by the mechanosensory machinery plays an important role in vascular endothelial signaling, referred to as WSS-induced mechanotransduction. The putative endothelial WSS mechanosensory complex is comprised of the platelet endothelial cell adhesion molecule-1 (PECAM-1), VE-cadherin, vascular endothelial growth factor receptor 2 (VEGFR2), and other molecules, primarily localized to the endothelial cell junction [52]. We previously demonstrated that PECAM-1 directly senses temporal changes in WSS [5] and others have shown that VE-cadherin acts as an adaptor in this process [52]. Junctional adhesion molecule-A (JAM-A/F11R) is an integral component of the endothelial cell junction complex with pleiotropic functions in cell physiology and development [14]. JAM-A/F11R plays a regulatory role in leukocyte-endothelial interaction, barrier function, and cell polarization [15]. Recent studies found that JAM-A/F11R also plays a role in mechanosensing via its interaction with zonula occludens-1, small G-proteins RhoA, and RhoGEF [41, 49]. Notably, other studies have shown that aging alters the function of JAM-A/F11R owing to its reduced tissue expression levels [45, 50]. In this context, we recently reported increased activity of A disintegrin and metalloproteinase, ADAM17 (also known as TNF converting enzyme or TACE), in adipose tissue arteries of older humans and aged mice [13], and what we found contributes to TNF-mediated remote vascular dysfunction. Interestingly, ADAM17 mediates proteolytic shedding of several other membrane-bound molecules, including JAM-A/F11R [19]. In this context, a previous in vitro study showed that activation of ADAM17 is associated with proteolytic release of JAM-A/F11R from endothelial cells [27]. Based on the aforementioned, the present study was designed to test the specific hypothesis that aging-related ADAM17 activation and increased JAM-A/F11R shedding impairs endothelial cell WSS mechanosensing thereby contributing to abnormal, lumen narrowing remodeling of small resistance arteries.

Methods

Animal characteristics

The work involving experimental animals was conducted under the protocol approved by the Institutional Animal Care and Use Committee at Medical College of Georgia, Augusta University. All experimental animal procedures performed in this study were in compliance with the European Convention for the Protection of Vertebrate Animals used for Experimental and other Scientific Purposes. Experiments were carried out in 28–30-month-old aged male

C57BL/6 J mice (obtained from the National Institute on Aging, Aged Rodent Colonies) and 12-week-old male C57BL/6 J mice (Jackson Laboratory). The aged mouse (28–30-month-old) is equivalent for older humans around 80 years, whereas the 3-month-old mouse is equivalent for 20-year-old humans. The mice were housed in the animal care facility and accessed rodent chow and tap water ad libitum with a 12-h light:dark cycle. Blood pressure (BP) was measured in conscious mice by tail-cuff plethysmography with a CODA Monitor noninvasive blood pressure system (Kent Scientific). Peak systolic blood flow velocity was measured non-invasively by pulsed wave Doppler imaging using a small animal ultrasound system (Vevo 3100, Visualsonics), similar as described before [25, 57].

Videomicroscopic assessment of isolated skeletal muscle arteries of the mouse

Mice were anesthetized with isoflurane (1–4%). Under deep anesthesia, the gracilis muscle was removed and placed in ice-cold calcium free Krebs solution (in mmol/L): 110.0 NaCl, 5.0 KCl, 1.0 $MgSO_4$, 1.0 KH_2PO_4, 5.5 D-glucose, and 24.0 $NaHCO_3$, equilibrated with a gas mixture of 10% O_2–5% CO_2-balanced nitrogen, at pH 7.4. Mice were euthanized by exsanguination and removal of the aorta and other vital organs were used for further assessments.

With the use of microsurgical instruments and an operating microscope, the gracilis muscle artery running intramuscularly was isolated and transferred into an organ chamber containing two glass micropipettes filled with calcium free Krebs solution. The artery was cannulated at both ends and the micropipettes were connected with silicone tubing to a hydrostatic reservoir to set the intraluminal pressure to 70 mmHg, and incubated for a 1-h period. Using videomicroscopy, the inner diameter, wall thickness, and wall to lumen ratio of the arteries were measured at an intraluminal pressure of 20 to 100 mmHg in 20 mmHg increments in the absence of extracellular calcium (calcium free Krebs solution) with a videocaliper (Colorado) [4, 16]. The wall/lumen ratio was calculated as $WT/D \times 100$, where WT is the wall thickness and D is lumen diameter, wall cross-sectional area (CSA) was calculated as: $CSA = p\ [D + 2WT/2]2 - p\ (D/2)2$, wall stress $(s) = P \times D/2WT$, where P is pressure and 1 mmHg = 1334 dyne/cm^2, as described [34].

In calcium-containing Krebs solution, spontaneous arterial tone developed in response to 70 mmHg pressure. Diameter changes were measured in response to cumulative concentrations of endothelium-dependent agonists, acetylcholine (ACh, 10^{-9}–10^{-6} M, Sigma), to the direct NO donor, sodium nitroprusside (SNP, 10^{-9}–10^{-5} M, Sigma), and to the calcium ionophore, A23187 (10^{-9}–10^{-6} M, Sigma). WSS-induced dilation of isolated arteries was assessed. Intraluminal flow was induced by changing perfusion pressure with an equal degree but in the opposite direction, in a stepwise manner (pressure difference, ΔP: 20 mmHg, 40 mmHg, 60 mmHg, 80 mmHg, and 100 mmHg). Flow was measured with a ball-type flow meter (Omega). Increases in intraluminal flow (from ~ 2 to ~ 20 µL/min) resulted in increases in wall shear stress (WSS, from ~ 2 to ~ 55 dyne/cm^2). WSS was calculated from the formula: $WSS = 8 \times Vm/D \times P$, where Vm is the mean fluid velocity, D is the lumen diameter, P is the viscosity (0.01 for Krebs solution). Vm is calculated using the formula: $Q = Vm*\eta*D2/4$, where Q is the flow rate and D is the lumen diameter.

Western immunoblotting

The skeletal muscle artery was isolated and homogenized in radio-immunoprecipitation assay (RIPA, Sigma) buffer mixed with 1% protease inhibitor cocktail (Sigma). Protein concentration was measured by Bradford assay. In other experiments, cultured endothelial cells and cell supernatants were collected and homogenized with RIPA buffer. Equal amounts of protein was loaded for gel electrophoresis. After blotting, membranes (Hybond-P, GE Healthcare) were probed with rabbit polyclonal anti-ADAM17 antibody (1:1000, ab2051, Abcam), goat anti-mouse JAM-A/F11R antibody (1:1000, AF1077, R&D Systems), or goat anti-human JAM-A/F11R (1:1000, AF1103, R&D Systems) followed by incubation with HRP linked secondary antibodies (anti-rabbit IgG, 7074S, Cell Signaling or anti-goat IgG, 811,620, Invitrogen). Enhanced chemiluminescence was visualized autoradiographically by ChemiDoc XRS + (Bio Rad). Protein expression was normalized for the total loaded protein using a BIO-RAD TGX Stain-Free

FastCast Acrylamide Kit (Cat. # 1,610,183), Chemi-Doc imaging system, and Image Lab Software (Bio Rad).

Histology, immunohistochemistry, immunocytochemistry, and en face immunofluorescence

Skeletal muscle samples were fixed in 4% paraformaldehyde (Affymatrix) and were embedded in paraffin. Sections were cut (8 µm) and re-hydrated through sequential incubations in a series of graded xylene, ethanol, and phosphate buffer solution (PBS). Antigen retrieval was performed by running slides submerged in IHC-TekTM Epitope Retrieval Solution. Slides were blocked with 15% horse serum (Vector Laboratories) for 1 h and followed by incubation with anti-ADAM17 antibody (1:100, ab2051, Abcam) or anti-mouse JAM-A/F11R antibody (1:100, AF1077, R&D) overnight at 4 °C. Fluorescent labeling was performed with Alexa Fluor® 546 conjugated donkey anti-rabbit IgG (1:250, A10040, Invitrogen) or Alexa Fluor® 647 conjugated donkey anti-goat IgG secondary antibody (1:250, ab150131, Abcam) for 1 h. DAPI (Vector Laboratories) was used for nuclear staining. Structured illumination microscopy (SIM-Apotome, AxioImagerM2, CarlZeiss) was used for immunofluorescent detection.

Sections were also processed for Elastin-Verhoeff Van Gieson (VVG) staining (Abcam). To measure the media thickness of arteries, we used systematic random sampling and unbiased measurements by employing the orthogonal intercept method (Stereo Investigator, MBF Bioscience). We made an average of 11 measurements for each blood vessel between the internal and external elastic lamina at each intercept of the randomly positioned stereology probe, and the estimated harmonic mean thickness was reported.

For immunocytochemistry, human umbilical vein endothelial cells (HUVECs) were grown onto collagen-coated glass coverslips and subsequently fixed with 4% paraformaldehyde. Unspecific antibody binding was blocked with 2% BSA in PBS for 1 h. Cells were incubated with goat anti-human JAM-A/F11R IgG antibody (1:200, AF1103, R&D) or VE-cadherin (1:200, D87F2, Cell Signaling) overnight at 4 °C. Alexa Fluor® 647 conjugated donkey anti-goat IgG (1:250, ab150131, Abcam) and Alexa Fluor® 488 conjugated donkey anti-rabbit IgG (1:250, SA5-10,038, Invitrogen) were added for 1 h. DAPI (Vector Laboratories) was used for nuclear staining. Structured illumination microscopy (SIM-Apotome, AxioImagerM2, CarlZeiss) was used for immunofluorescent detection.

En face immunofluorescence staining was performed as described before [26]. In brief, mice were anesthetized with isoflurane (1–4%). Under deep anesthesia, saline solution containing heparin (40 U/mL) was perfused into the apex of the left ventricle by inserting a 26 G needle attached to a gravity perfusion (120 cm H_2O) followed by 4% paraformaldehyde in PBS. The aorta was harvested and isolated, and cut longitudinally. Then, the aorta was permeabilized by 0.1% Triton X-100 in PBS for 10 min at room temperature and blocked with 10% horse serum (Vector Laboratories) in Tris-buffered saline with 2.5% Tween 20, for 30 min at room temperature. The aorta was incubated with goat anti-mouse JAM-A/F11R antibody (1:50, AF1077, R&D Systems) and rabbit anti-mouse VE-cadherin antibody (1:50, ab33168, Abcam) overnight at 4 °C. The aorta was then incubated with secondary antibodies (1:250, Alexa Fluor® 647 conjugated donkey anti-goat IgG, ab150131, Abcam; Alexa Fluor® 546 conjugated donkey anti-rabbit IgG, A10040, Invitrogen) for 1 h at room temperature. Structured illumination microscopy (SIM-Apotome, AxioImagerM2, CarlZeiss) was used for immunofluorescent detection.

In vivo confined arterial overexpression of mouse ADAM17 or ADAM17 cleavage resistant mutant mouse JAM-A^{V232Y}

Recombinant adeno-associated virus (AAV9) and adeno-associated virus 2-QuadYF (AAV2QuadYF) were constructed and purchased from VectorBuilder. Mouse ADAM17-mCherry-AAV9 was used to selectively overexpress ADAM17 in arteries of 12-week-old mice (young). Overexpression eGFP-AAV9 was used for controls. In addition, mutant mouse JAM-A^{V232Y}-mCherry-AAV2QuadYF (mtJAM-A^{V232Y}) was used to overexpress ADAM17 cleavage resistant mutant mouse JAM-A in arteries of 30-month-old mice (aged). Mice were anesthetized with isoflurane (1–4%) and the left femoral artery segment proximal and distal to the gracilis muscle artery was exposed and temporarily clamped using microvascular clips (depicted in Fig. 4a). A glass capillary (opening

tip ~ 2 μm) containing the AAV particles (5×10^9 AAV diluted in 10 μL sterile PBS) was then connected to a pneumatic drug ejection system (PDES-02TX, NPI). Using a micromanipulator (U-31CF, Narishige), the AAV particles were microinjected into the femoral artery. After 30 min, microvascular clamps were released from the femoral artery and the skin was closed with wound closure clips. After 2 weeks, mice were anesthetized with isoflurane (1–4%) and were euthanized by exsanguination, the left (ipsilateral) and right (contralateral) femoral and gracilis arteries were dissected and used for experiments, as described above. Protein expression of ADAM17, mCherry, and eGFP were detected in ipsilateral (left) and contralateral (right) arteries using Western immunoblots by using anti-ADAM17, anti-mCherry (1:1000, 43590S, Cell Signaling), or anti-eGFP (1:1000, 2956S, Cell Signaling) antibodies. Exogenous, AAV9-delivered ADAM17 expression in the arterial endothelium was also confirmed by mCherry immunofluorescent labeling.

Endothelial cell culture under flow condition

Human umbilical vein endothelial cells (HUVECs) were purchased from PromoCell (Heidelberg, Germany). HUVECs were cultured in endothelial cell growth medium 2 and used between 4 and 10 passages. WSS was applied to confluent HUVECs using an Ibidi pump system (Ibidi, Germany). HUVECs (10^5 cells/slide) were seeded onto IbiTreat μ-slides $I^{0.6}$ or IbiTreat μ-slides $I^{0.4}$ (Ibidi) and placed in an incubator at 37 °C with 5.0% CO_2. The Ibidi pump system and proprietary software was used to control the level of WSS applied to cells by controlling total media flow rate through the channels of known dimensions. HUVECs were cultured under defined WSS (0, 4, 8, 16, and 32 dyne/cm^2) for 48 h or 72 h. Phase contrast microscopy was used to collect images of HUVECs every 24 h. The ImageJ directionality plugin or angle measurement tool was then used to measure cell orientation angle distribution relative to the flow direction. The average cell orientation angle was also calculated. In separate experiments, transfection of HUVECs with JAM-A/F11R small interfering RNA (siRNA, Dharmacon™) was carried out using Lipofectamine® RNAiMAX Transfection Reagent (ThermoFisher Scientific). HUVECs were cultured with recombinant human ADAM17 (R&D Systems) or Phorbol 12-Myristate 13-Acetate (PMA, 100 nM for 2 h, Cayman Chemicals). HUVECs were then cultured under defined WSS (8 dyne/cm^2) for 72 h.

Site-directed mutagenesis

Human JAM-A/F11R plasmid (#70,073, Addgene, Cambridge, MA) was used as a template for site-directed mutagenesis. Mutations were introduced with Q5® Site-Directed Mutagenesis Kit (New England Biolabs, Ipswich, MA). Mutagenic primers were designed individually and ordered from Integrated DNA Technologies (Coralville, IA). A mutant with gain of restriction site (V232Y) encoded by proximal non-conservative missense mutations was generated (Supplementary Fig. 2). Sequences were as follows, valine to tyrosine at 232: CATGGAAGCTTATGA GCGGAATGTGGG and CGCACAGCATTTGAA GTC. Mutant strands were synthesized according to the manufacturer's protocol and proceeded immediately to transformation. Aliquots of *E. coli* XL10-Gold ultracompetent cells were transformed with the amplified plasmid DNA. All constructs were checked by restriction site mapping and sequencing. Aliquots of Mix & Go competent cells (Strain Zymo 5) were incubated with the wild type and mutant plasmids for 5 min on ice. The cells were spread on LB-agar plates containing the appropriate antibiotic (Ampicillin) for the plasmid vector and incubated overnight (16–18 h) at 37 °C. The plasmids were isolated with the Zymo-PUREII Plasmid Maxi kit (Zymo Research, Irvine, CA). Transfection of HUVECs with hJAM-A or mtJAM-A^{V232Y} was carried out using Lipofectamine 3000 Transfection Reagent (ThermoFisher Scientific). Transfected HUVECs were then cultured under defined WSS (8 dyne/cm^2) for 72 h and cell orientation angle distribution relative to the flow direction was measured as above.

Statistical analysis

All statistical analyses were performed using GraphPad Prism Software. Data were drawn to analyze after being tested for and meeting normality using the Kolmogorov–Smirnov test. Data comparisons between groups repeatedly over time were analyzed by two-way repeated-measures of ANOVA followed by Sidak's post-hoc test for multiple comparisons or with two-tailed, unpaired Student

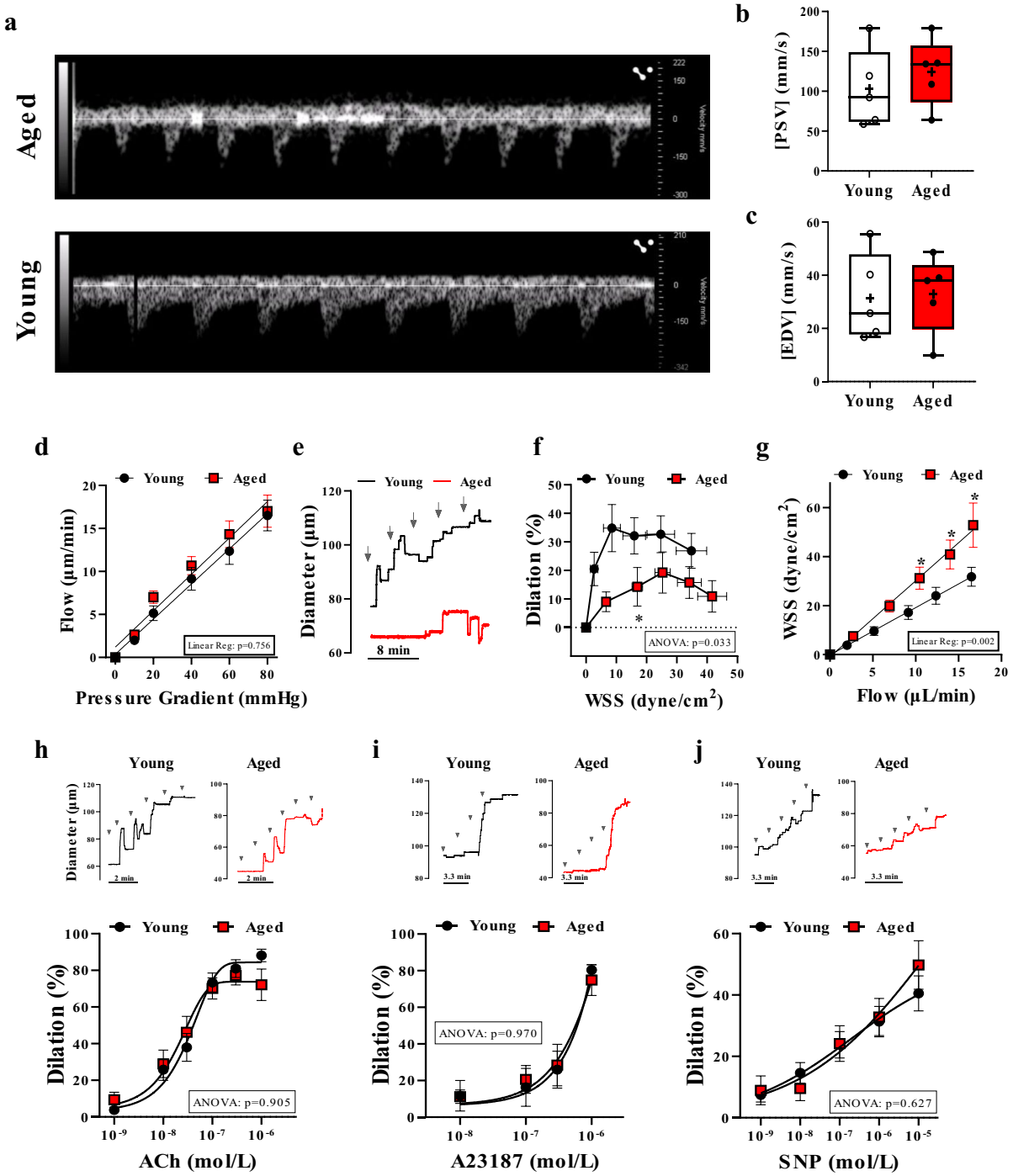

t test, as appropriate. Data are expressed either as mean ± SEM or box-and-whisker plots, in which the minimum, the 25th percentile, the median, the 75th percentile, and the maximum are presented, and + indicates the mean of values. $P < 0.05$ was considered statistically significant.

◂**Fig. 1** Impaired flow/WSS-induced dilation in skeletal muscle arteries of aged mice. Representative images (**a**) and summary data of peak systolic velocity (PSV, **b**) and end diastolic velocity (EDV, **c**) measured by Doppler ultrasound in the femoral artery from aged and young mice ($n = 5$ in each group). **d**–**g**. Stepwise increases in the pressure gradient induced a similar increase in intraluminal flow of isolated skeletal (m. gracilis) arteries in aged and young mice (**d**). Representative original traces (**e**) and summary data (**f**) of percent changes in diameter of arteries in response to increased WSS in young vs. age mice. Flow–WSS relationship is shown on Panel **g**. Representative original traces and summary data of percent diameter changes of isolated arteries in response to cumulative concentrations of acetylcholine (ACh, 10^{-9} to 10^{-6} mol/L) (**h**), Ca^{2+} ionophore, A23187 (10^{-9} to 10^{-6} mol/L) (**i**) or NO donor, sodium nitroprusside (SNP, 10^{-9} to 10^{-5} mol/L) (**j**) in young and aged mice. Arrows indicate stepwise increasing of flow or administration of agonists. Data are mean ± SEM or presented as box-and-whisker plots, in which the minimum, the 25th percentile, the median, the 75th percentile, and the maximum are shown, + indicates the mean of values. For statistical analyses of data on Student's *t* test, repeated measures two-way ANOVA (insets: ANOVA p value for age effect is shown) with Sidak multiple comparisons were used. $^*p < 0.05$ young vs. aged

Results

Impaired WSS response and hypertrophic inward remodeling in arteries of aged mice

Previous studies have shown that vascular remodeling develops in animal models of aging [21, 30, 31, 33, 34]. To address whether biomechanical forces are linked to aging-related vascular remodeling, we measured blood pressure and femoral artery blood flow as well as used videomicroscopy to assess both functional and structural properties of isolated, cannulated, and pressurized mouse skeletal (m. gracilis) muscle arteries. Comparable systolic and diastolic blood pressure was observed between young (12-week-old) and aged (30-month-old) mice (young vs. aged in mmHg, systolic pressure: 113 ± 6 vs. 95 ± 8 and diastolic pressure: 90 ± 4 vs. 79 ± 8, not significant). Also, no significant change in peak systolic blood flow velocity in the femoral artery was found in aged mice (Fig. 1a–c).

We assessed WSS-induced vasodilation in isolated and pressurized skeletal muscle arteries of young and aged mice. Using videomicroscopy, we measured diameter changes in arteries subjected to stepwise increases in intraluminal flow which was generated by a stepwise increase in pressure gradient in the inflow and outflow cannulas. The applied pressure gradients induced a same level of intraluminal flow in arteries of young and aged mice (Fig. 1d). We found, however, that WSS-induced vasodilation was not only reduced in magnitude (Fig. 1e, f) in aged mice, but the maximum dilator response required significantly higher WSS levels (~ 25 dyne/cm^2) when compared to younger mice (~ 10 dyne/cm^2) (Fig. 1f). At any given flow rate, the calculated WSS remained significantly higher in arteries of aged mice (Fig. 1g). No significant difference in the vasodilation response to the endothelium-dependent agonist, acetylcholine (Fig. 1h), the calcium ionophore, A23187 (Fig. 1i), or the endothelium-independent agonist, direct nitric oxide donor, sodium nitroprusside (Fig. 1j), was noted between young and aged mice.

We also found that small skeletal muscle arteries isolated from aged mice displayed a reduced internal diameter compared to young animals, as measured at intraluminal pressure ranges between 20 and 100 mmHg (Fig. 2a, b). Arteries from aged mice had increased pressure-wall thickness, pressure-wall thickness/lumen ratio, and pressure-cross-sectional area relationships, when compared with young animals (Fig. 2c–e). The calculated wall stress/pressure relationship was reduced in aged arteries, compared to the young (Fig. 2f). Histological sections from aged (vs. young) mice showed increased media thickness of gracilis muscle arteries (Fig. 2g, h). Together, these data demonstrate that impaired WSS response is associated with inward hypertrophic remodeling [33] in the skeletal muscle resistance arteries of the aged mice.

ADAM17 reduces endothelial cell junction localized JAM-A/F11R in aged mice

Similar to our previous study performed in the adipose tissue in older adults and in aged mice [13], we have detected ADAM17 expression in the skeletal muscle arterial wall, including the endothelial cells, in both young and aged mice (Fig. 3a). We found that ADAM17 protein expression was significantly upregulated in skeletal muscle arteries from aged mice compared to young (Fig. 3b). Endothelial cells also expressed JAM-A/F11R, an ADAM17 cleavage substrate, with no change in total protein expression levels in young and aged mice (Fig. 3a, b).

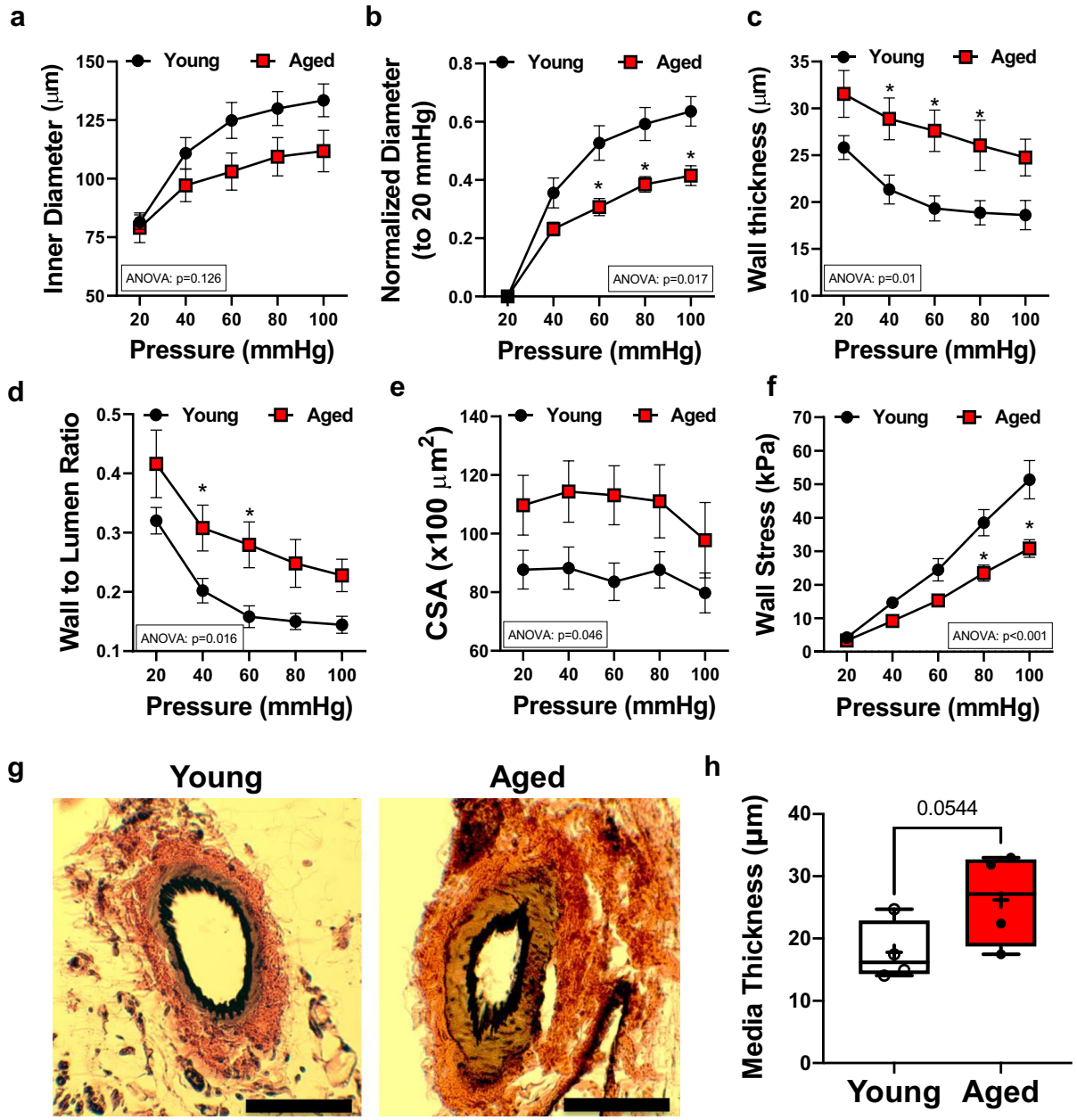

Fig. 2 Hypertrophic inward remodeling in skeletal muscle arteries of aged mice. Skeletal muscle (m. gracilis) artery lumen diameter and vascular wall characteristic in response to increases in intraluminal pressure, ex vivo. Inner diameter (**a**), normalized diameter (to initial diameter at 20 mmHg) (**b**), wall thickness (**c**), wall-to-lumen ratio (**d**), cross-sectional area (CSA) (**e**), and calculated wall stress (**f**) in relation to increases in intraluminal pressure from 20 to 100 mmHg in skeletal muscle arteries isolated from young ($n=9$) and aged ($n=6$) mice. Data are mean ± SEM. For data analyses on panelse (**a**–**h**), repeated measures two-way ANOVA (insets: ANOVA p value for age effect is shown) with Sidak multiple comparisons were used. *$p<0.05$ young vs. aged. Representative microphotographs of Elastin Verhoeff Van Gieson staining (EVG, elastic fibers and nuclei being stained black, collagen stained red, and cytoplasmic elements stained yellow/brown, scale bar: 50 µm) (**g**). Media thickness of arteries was measured by an unbiased orthogonal intercept method (Stereo Investigator, MBF) (**h**). Data are presented as box-and-whisker plots, in which the minimum, the 25th percentile, the median, the 75th percentile, and the maximum are shown, + indicates the mean of values. For statistical analyses of data on panel h, Studentis t test was used

Previously, ADAM17 activation was shown to alter the subcellular localization of JAM-A/F11R via regulated cleavage [27]. To determine aging-related changes in endothelial cell distribution of JAM-A/F11R, we performed *en face* immunostaining in the aorta of young and aged mice. JAM-A/F11R was more widely distributed in endothelial cells of aged mice that also had irregular borders of the cell junction (Fig. 3c, d). The level of endothelial cell junction-localization of JAM-A/F11R, relative to VE-cadherin, was significantly reduced in aged mice (Fig. 3e). We also noted that the endothelial nuclei in the aorta of aged mice were less elongated than those in young mice (nuclei aspect ratios, Fig. 3f). Given that fluid WSS causes endothelial cells and their nuclei to elongate [48], this data also indicated altered arterial WSS-induced signaling in the aged animals.

The relative abundance of JAM-A/F11R localized to endothelial cell junctions was also assessed in HUVECs cultured under flow conditions before and after ADAM17 activation. To activate ADAM17, we treated endothelial cells with phorbol-myristate-acetate (PMA), as one of the strongest activators of ADAM17 [17, 51, 55, 56]. HUVECs were subjected to flow (WSS = 8 dyne/cm^2, for 48 h) with or without treatment with PMA (100 nM for 2 h). We found that PMA reduced the expression of junction localized JAM-A/F11R, without significantly altering the nuclei aspect ratios (Fig. 3i, j).

Focal, in vivo, overexpression of ADAM17 impairs WSS response and induces vascular remodeling in arteries of young mice

To specifically assess the impact of ADAM17 on the WSS response and subsequently developed arterial remodeling in vivo, the adeno-associated virus 9 (AAV9) encoding mouse ADAM17 (labeled with mCherry, for controls AAV9 encoding eGFP) was microinjected focally into the lumen of the left (ipsilateral) skeletal muscle artery (Fig. 4a). After 2 weeks, from confined intra-arterial delivery of the ADAM17 AAV9 vector, we found that ADAM17 expression was significantly augmented in the injected, ipsilateral artery, but not in the contralateral artery (Fig. 4b, c). Delivery of eGFP-AAV9, which served to control for injection-induced injury, had no effect on ADAM17 expression (Fig. 4b).

We found that overexpression of ADAM17 in the arteries of young mice significantly reduced the magnitude of WSS-induced dilation without affecting agonist, acetylcholine- and calcium-ionophore, A23187-induced responses (Fig. 4e, f). Similar to responses from aged arteries, in ADAM17-overexpressed arteries WSS-induced vasodilation reached its maximum only at higher WSS levels (~20 dyne/cm^2) compared to the contralateral artery or the eGFP-overexpressed blood vessel (~5–10 dyne/cm^2) (Fig. 4d, g). In addition, the impaired WSS response after ADAM17 overexpression was accompanied by increased arterial wall thickness and increased wall-to-lumen-pressure relationship, with no significant changes observed in the inner arterial lumen diameter-pressure relationship (Fig. 4j–o).

ADAM17 activation or deletion of JAM-A/F11R impairs WSS-induced endothelial cell alignment

Next, we investigated the underlying mechanisms by which ADAM17 impairs WSS mechanosensing in endothelial cells. Cultured HUVECs were subjected to steady laminar flow at various WSS levels, from 0 to 32 dyne/cm^2, over 3 days. Endothelial cell alignment, a measurement of the ability of endothelial cells to sense and respond to WSS, was quantified by measuring the angle between the major endothelial cell axis and the direction of flow. In response to WSS conditions, endothelial cells displayed an elongated morphology and aligned with the direction of flow; maximum cell alignment (i.e., lowest angle deviation from flow direction) was reached at a WSS of 8 dyne/cm^2 (Supplementary Fig. 1). Consequently, endothelial cell alignment (under flow conditions, WSS 8 dyne/cm^2 for 3 days) was measured in HUVECs subjected to recombinant ADAM17 protein or transfected with JAM-A/F11R targeted siRNA or scrambled control siRNA. While ADAM17 exposed or JAM-A/F11R depleted endothelial cells displayed an elongated morphology, they failed to align in the direction of flow during the 3-day culture period compared to control siRNA transfected HUVECs (Fig. 5).

Endothelial cells expressing the ADAM17 cleavage resistant JAM-A/F11R align to flow direction

To address whether JAM-A/F11R is a direct substrate for ADAM17, we employed site-directed mutagenesis

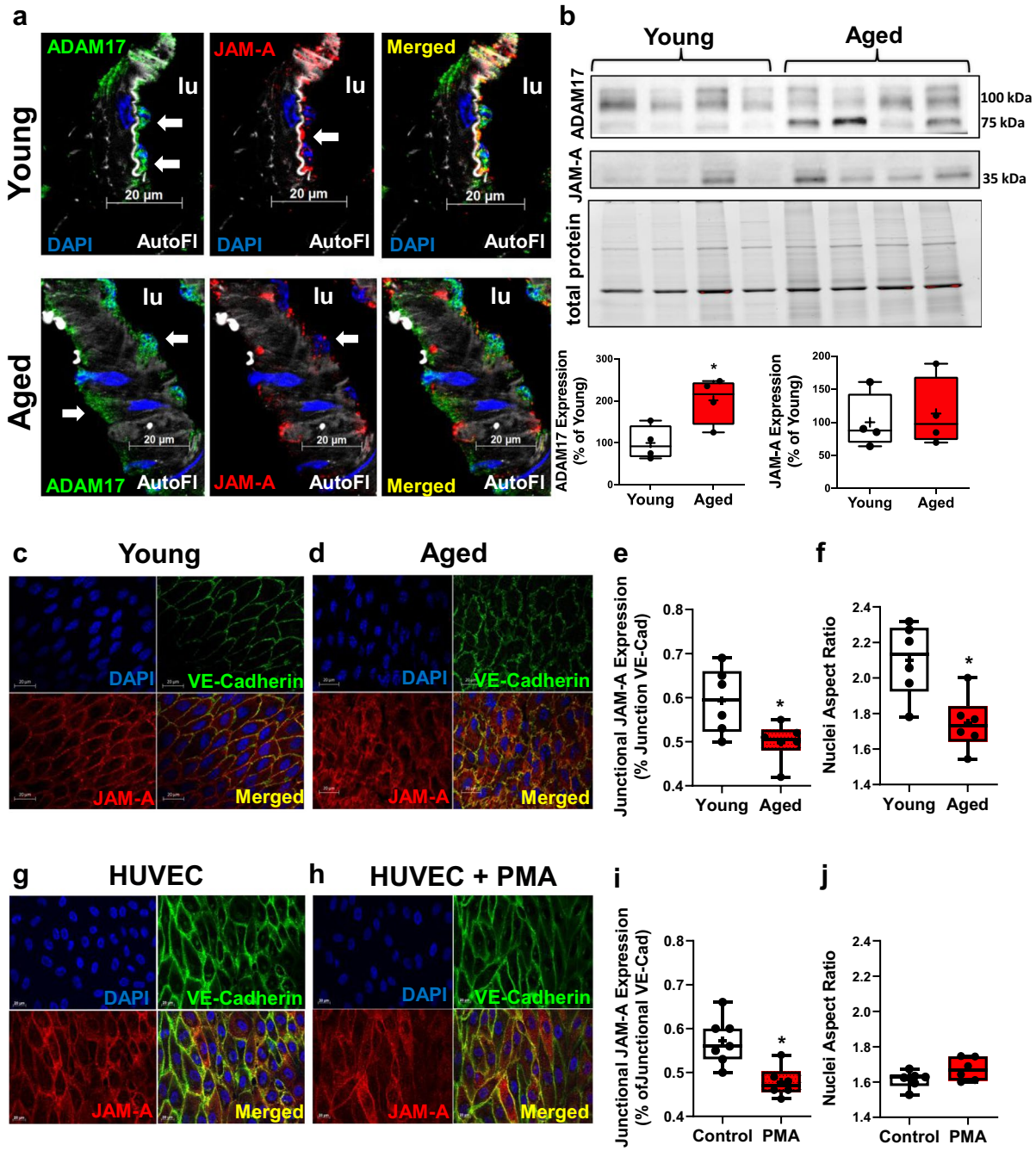

to generate an ADAM17 cleavage resistant human JAM-A/F11R. HUVECs were transfected with either wild-type JAM-A (wtJAM-A) or mtJAM-A^{V232Y} and were subjected to flow (3 days at WSS 8 dyne/cm^2) with or without recombinant ADAM17. In HUVECs expressing wtJAM-A, we detected an increased abundance of the cleaved form of JAM-A/F11R, regardless of ADAM17 exposure. However, we noted that the conditioned media of mtJAM-A^{V232Y} expressed HUVECs contained significantly reduced JAM-A/F11R levels than that of wtJAM-A expressing cells (Supplementary Fig. 2). Both wtJAM-A and mtJAM-A^{V232Y} expressing HUVECs displayed an elongated morphology and aligned to the direction of flow

◂ **Fig. 3** Increased ADAM17 expression is accompanied by reduced endothelial cell junction localized JAM-A/F11R. Representative microphotographs for immunofluorescent staining for ADAM17 (shown in green, white arrow) and JAM-A/F11R (shown in red, white arrow) in skeletal muscle arteries of young ($n=3$) and aged ($n=3$) mice (scale bar: 20 µm). Nuclei were stained with DAPI (blue). Elastic lamina interna is shown as autofluorescence (AutoFl, in white). Lumen of the artery: lu (**a**). Representative images of Western immunoblot and summary data (for protein expression of ADAM17 and JAM-A/F11R in skeletal muscle arteries obtained from young ($n=4$) and aged ($n=4$) mice (**b**). Representative microphotographs of *en face* staining of JAM-A/F11R (shown in red) and VE-cadherin (show in green) in the aorta from young ($n=6$) and aged mice ($n=6$) (**c**, **d**). Immunocytochemistry of JAM-A/F11R (red) and VE-cadherin (green) in HUVECs cultured under flow conditions (WSS = 8 dyne/cm^2, for 48 h) with or without treatment with phorbol myristate acetate (PMA, 100 nM, acute treatment for 2 h) (**g**, **h**). Nuclei were stained with DAPI (blue) and merged images are also shown. Scale bars: 20 µm. Pearson's correlation analyses of relative colocalization of JAM-A/F11R and VE-cadherin expression, measured at cell junctions (**e**, **i**). Summary data of the nuclei aspect ratio as calculated using the long and short axis of the nuclei (**f**, **j**). Data are presented as box-and-whisker plots, in which the minimum, the 25th percentile, the median, the 75th percentile, and the maximum are shown, + indicates the mean of values. For statistical analyses of data Studentati*t* test was used. *$p<0.05$ young vs. aged

during the 72-h culture period (Fig. 6a, b, Fig. 6e–g). These data indicate that the mutated JAM-A/F11R does not alter the normal WSS response. We found that wtJAM-A expressing cells subjected to recombinant ADAM17 elongated but failed to efficiently orient to the direction of flow (Fig. 6c, e, h). In contrast, mtJAM-A^{V232Y} expressing HUVECs were elongated and aligned, even in the presence of ADAM17 (Fig. 6d, e, i). These results underscore a specific defect in the WSS sensing mechanism by which wild-type JAM-A/F11R expressing cells align to the direction of flow after ADAM17 exposure, which is rescued by the ADAM17 cleavage resistant mtJAM-A^{V232Y}.

Focal, in vivo, overexpression of ADAM17 cleavage resistant mutant mouse JAM-A^{V232Y} improves the WSS response, but does not reverse abnormal remodeling in aged mice

To determine if aging-associated impairment of WSS mechanosening and abnormal arterial remodeling can be reversed, the AAV2QuadYF encoding an ADAM17 cleavage-resistant mutant mouse JAM-A/F11R (mtJAM-A^{V232Y} AAV2QuadYF, labeled with mCherry) was microinjected focally into the lumen of the left (ipsilateral) skeletal muscle resistance artery of the 30 months, aged mice. After 2 weeks of confined intra-arterial delivery of the mtJAM-A^{V232Y} AAV2QuadYF vector, we found that the targeted skeletal muscle resistance artery segment exhibited a significantly augmented WSS-induced dilation, whereas the endothelium-dependent agonist, ACh- and the direct NO donor SNP-induced responses remained similar when compared to contralateral artery of the aged mice (Fig. 7a–c). There were however no significant changes observed in the arterial wall thickness and wall-to-lumen-pressure relationship, as well as the inner arterial lumen diameter-pressure relationship in the mtJAM-A^{V232Y} overexpressed artery segments when compared to the contralateral artery of the aged mice (Fig. 7d–f).

Discussion

The present study aimed to test the hypothesis that aging-related impairment in WSS mechanosensing is the primary cause of abnormal remodeling in resistance arteries. Our results indicate that in aging, an upregulated ADAM17 expression impairs the vascular endothelial WSS mechanosensory process leading to a lumen narrowing, hypertrophic remodeling in skeletal muscle resistance arteries. In support, we provide in vivo and in vitro evidence showing that increased vascular expression of ADAM17, through an excess cleavage of endothelial JAM-A/F11R, is associated with impaired WSS-induced vasodilation and diminished WSS-dependent endothelial cell alignment. We conclude that aging-associated reduction in endothelial cell WSS mechanosensing and subsequently developed abnormal arterial remodeling is mechanistically linked to increased ADAM17-mediated excess cleavage of JAM-A/F11R, the newly described member of endothelial WSS mechanosensing.

In agreement with previous studies [21, 30, 34], our present study found that a prominent vascular remodeling occurs in aged mice. In skeletal muscle resistance arteries of aged mice, we observed a reduced luminal diameter, as well as increased wall thickness and wall to lumen ratio, measured at different intraluminal pressure levels (from 40 to

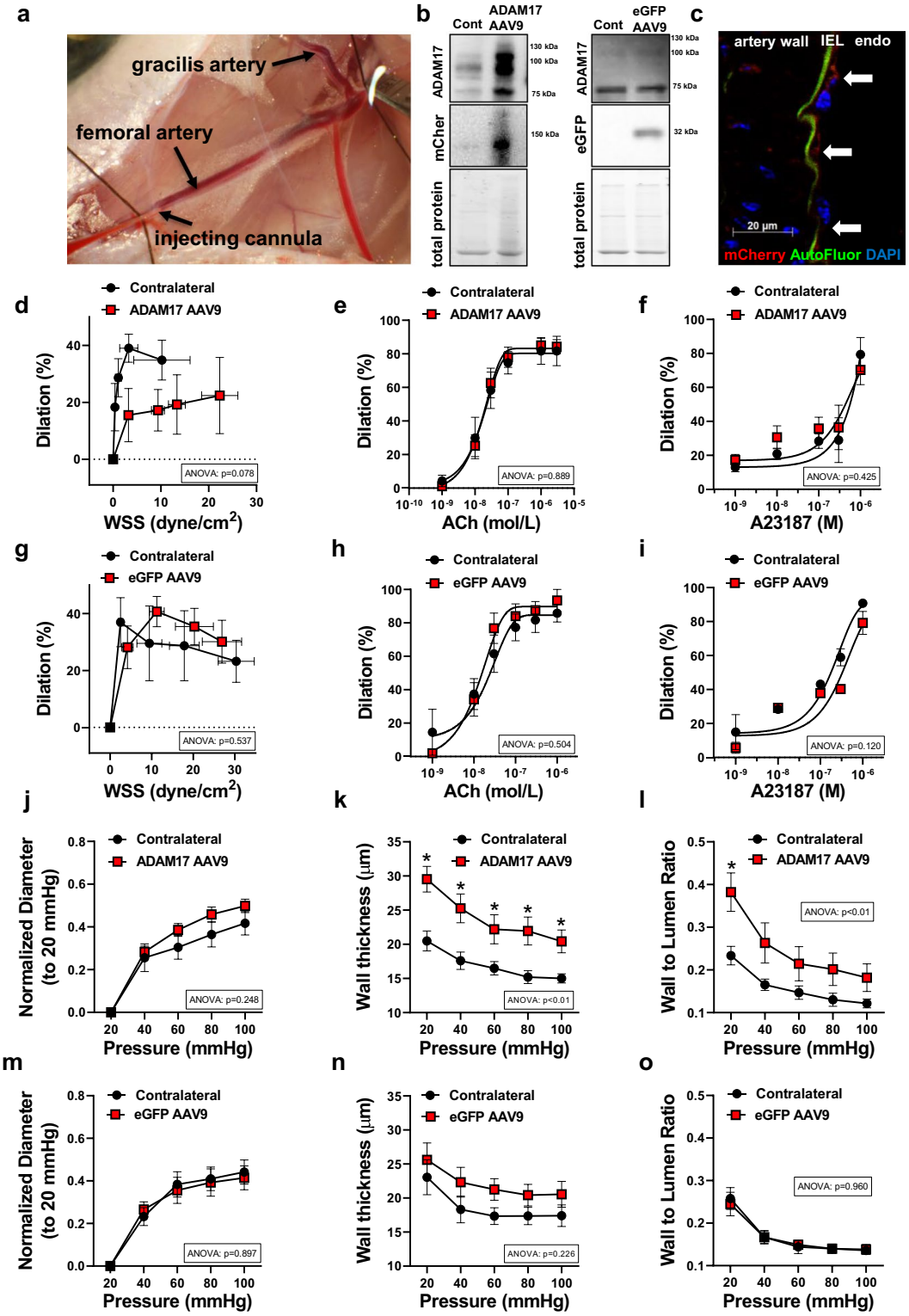
a
gracilis artery
femoral artery
injecting cannula
b
Cont
ADAM17 AAV9
ADAM17
mCher
total protein
130 kDa
100 kDa
75 kDa
150 kDa
Cont
eGFP AAV9
ADAM17
eGFP
total protein
130 kDa
100 kDa
75 kDa
32 kDa
c
artery wall
IEL
endo
20 µm
mCherry AutoFluor DAPI
d
Contralateral
ADAM17 AAV9
Dilation (%)
WSS (dyne/cm2)
ANOVA: p=0.078
e
Contralateral
ADAM17 AAV9
Dilation (%)
ACh (mol/L)
ANOVA: p=0.889
f
Contralateral
ADAM17 AAV9
Dilation (%)
A23187 (M)
ANOVA: p=0.425
g
Contralateral
eGFP AAV9
Dilation (%)
WSS (dyne/cm2)
ANOVA: p=0.537
h
Contralateral
eGFP AAV9
Dilation (%)
ACh (mol/L)
ANOVA: p=0.504
i
Contralateral
eGFP AAV9
Dilation (%)
A23187 (M)
ANOVA: p=0.120
j
Contralateral
ADAM17 AAV9
Normalized Diameter (to 20 mmHg)
Pressure (mmHg)
ANOVA: p=0.248
k
Contralateral
ADAM17 AAV9
Wall thickness (µm)
Pressure (mmHg)
ANOVA: p<0.01
l
Contralateral
ADAM17 AAV9
Wall to Lumen Ratio
Pressure (mmHg)
ANOVA: p<0.01
m
Contralateral
eGFP AAV9
Normalized Diameter (to 20 mmHg)
Pressure (mmHg)
ANOVA: p=0.897
n
Contralateral
eGFP AAV9
Wall thickness (µm)
Pressure (mmHg)
ANOVA: p=0.226
o
Contralateral
eGFP AAV9
Wall to Lumen Ratio
Pressure (mmHg)
ANOVA: p=0.960

◂ **Fig. 4** Impaired WSS mechanosensing and vascular remodeling after in vivo overexpression of ADAM17 in arteries of young mice. Representative photo depicts a procedure of intraarterial microinjection of ADAM17 encoded adeno-associated virus 9 (AAV9, labeled with mCherry) into the left skeletal muscle artery of the young mice (**a**). Representative images of Western immunoblot for detecting protein expression of ADAM17, mCherry, or eGFP in left (ipsilateral injected) and contralateral (Cont) skeletal muscle arteries are shown (**b**). Immunofluorescent staining for mCherry (shown in red, white arrow) was employed to confirm endothelial expression of the exogenous, AAV9 delivered ADAM17 in the left (ipsilateral) skeletal muscle arterial endothelium (endo). Interna elastic lamina (IEL) is shown in green with autofluorescence (AutoFluor). Nuclei were stained with DAPI (blue) (**c**). Summary data ($n = 6$–8, in each group) of percent diameter changes of isolated left ipsilateral (ADAM17 AAV9 or eGFP AAV9 injected) and right (contralateral) skeletal (m. gracilis) arteries in response to increased flow/WSS (**d**, **g**) or cumulative concentrations of acetylcholine (ACh, 10^{-9} to 10^{-6} mol/L) (**e**, **h**) and Ca^{2+} ionophore, A23187 (10^{-9} to 10^{-6} mol/L) (**f**, **i**). Summary data ($n = 6$–8, in each group) of inner normalized diameter (to initial diameter at 20 mmHg) (**j**, **m**), wall thickness (**k**, **n**), and wall-to-lumen ratio (**l**, **o**) in relation to increases in intraluminal pressure from 20 to 100 mmHg in isolated left ipsilateral (ADAM17 AAV9 or eGFP AAV9 injected) and right (contralateral) skeletal (m. gracilis) arteries. Data are mean ± SEM. For data analyses repeated measures two-way ANOVA (ANOVA p value for the corresponding effects are shown in the insets) with Sidak multiple comparisons were used. *$p < 0.05$ contralateral vs. ipsilateral artery

100 mmHg), whereas the calculated circumferential wall stress was reduced when compared to young mice. This implies that resistance arteries of aged mice undergo a hypertrophic inward vascular remodeling. Similar morphological changes are likely to occur in hypertension when the resistance artery is exposed to chronically elevated intraluminal pressure in an attempt to normalize circumferential stress. In this study, however, both systolic and diastolic arterial blood pressures tended to decrease with age, similar to previous reports [21, 30, 34], hence questioning the role of increased intraluminal pressure in contributing to aging-related abnormal remodeling of resistance arteries.

Previous studies have shown that a lumen narrowing arteriolar remodeling also develops in response to rapid cessation of intraluminal blood flow, which is accompanied by increased vascular smooth muscle cell proliferation and media thickening [8, 37]. On the other hand, an increase in blood flow induces outward, hypotrophic arterial remodeling [1, 2] and this is associated with recruitment of leukocytes and secretion of matrix metalloproteinases, cytokines, and extracellular matrix proteins [3, 32, 40, 43, 44]. In their study, Pistea et al. found that cessation of flow causes a rapid inward arterial remodeling in cultured coronary arteries, in the absence of tissue metabolites and blood-borne cells or chemokines [37]. The authors concluded that inward remodeling is likely to be mediated by the deficiency of flow-induced endothelial production of NO [37], which normally exerts vasodilator and antiproliferative effects on vascular smooth muscle cells. Indeed, previous studies have found that the NO agonist, acetylcholine (ACh)-induced dilation is reduced in femoral, carotid, and forearm conduit arteries in aged mice and humans, whereas endothelium-independent dilation to the NO donor, sodium nitroprusside (SNP) is not altered by age (Donato, J Physiol 2011; Gioscia-Ryan, J Physiol 2014). Similar findings were observed in the soleus muscle feeding artery in aged Fisher 344 rats (Trott et al. J Appl Phys 2009). Results from our present study however revealed no significant differences in ACh-, calcium ionophore A23187-, and SNP-induced dilations in skeletal muscle resistance arteries in aged and young mice. It should be noted that while in conduit vessels, NO, cGMP, and cGKI are the major effectors of the ACh response, the contribution of endothelium-dependent hyperpolarizing factor (EDHF)-mediated dilation is more prominent in resistance arteries (Koeppen et al. Hypertension 2004). Therefore, our results could be interpreted that EDHF-mediated dilation as well as the responsiveness to an exogenous NO donor are preserved in skeletal muscle resistance arteries of aged mice. It is however possible that an upregulated EDHF response compensates for the potentially impaired NO-mediated vasodilation, such as reported earlier in hypertension (Goto et al. Hypertension Research 2012), but this scenario was not systematically assessed in our current study.

Of note, in small resistance arteries, the major stimulus to initiate endothelial production of NO is the increase in wall shear stress [29]. Previous studies evaluating age-related changes in vascular endothelial function found that increases in flow results in a reduced dilation of isolated coronary resistance arteries in older adults [7] and in aged rats [9, 42]. Notably, in these studies, the authors did not calculate and

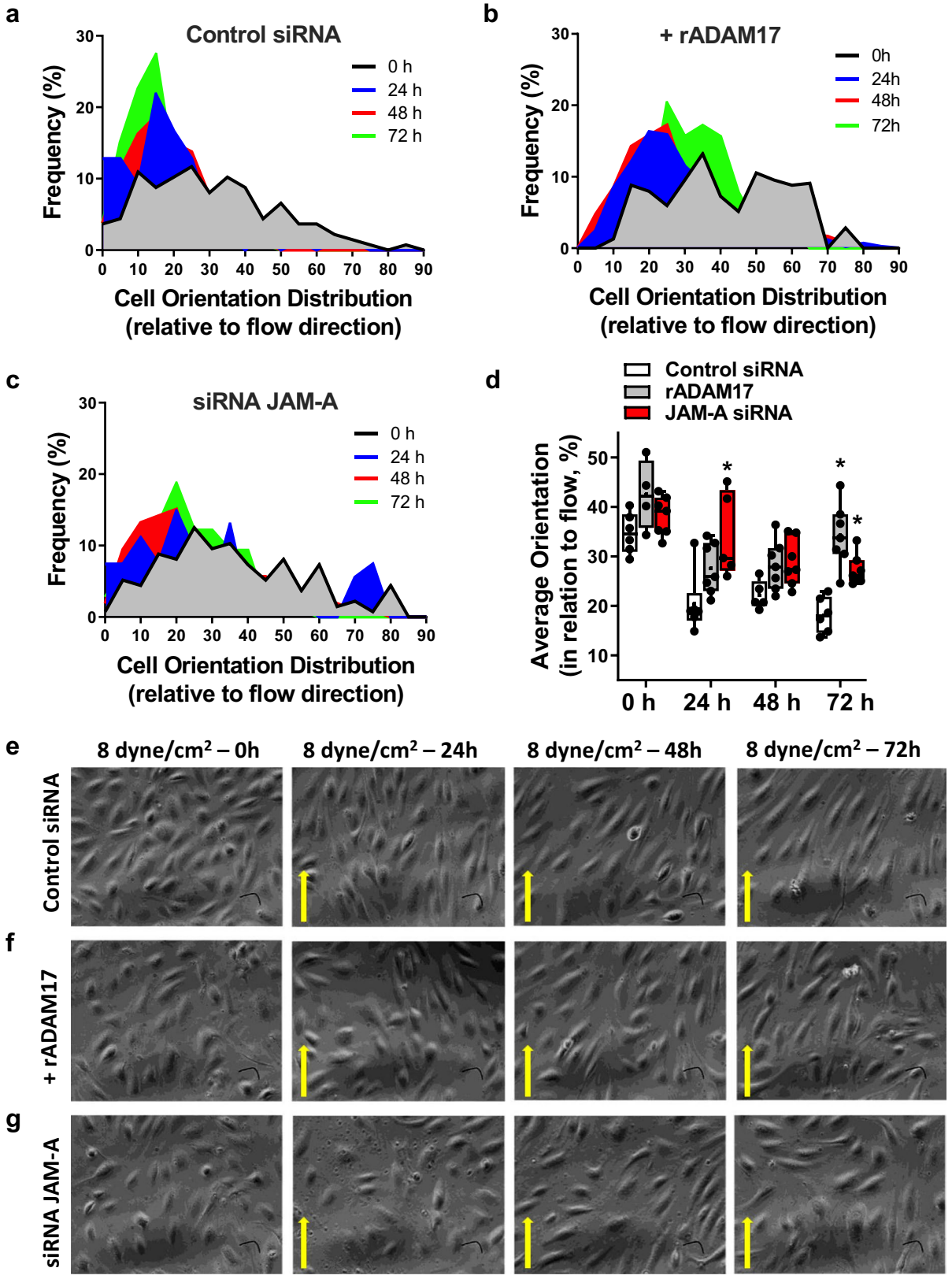
a
Control siRNA
Frequency (%)
0 h
24 h
48 h
72 h
Cell Orientation Distribution
(relative to flow direction)
b
+ rADAM17
Frequency (%)
0h
24h
48h
72h
Cell Orientation Distribution
(relative to flow direction)
c
siRNA JAM-A
Frequency (%)
0 h
24 h
48 h
72 h
Cell Orientation Distribution
(relative to flow direction)
d
Control siRNA
rADAM17
JAM-A siRNA
Average Orientation
(in relation to flow, %)
0 h
24 h
48 h
72 h
e
8 dyne/cm² – 0h
8 dyne/cm² – 24h
8 dyne/cm² – 48h
8 dyne/cm² – 72h
Control siRNA
f
+ rADAM17
g
siRNA JAM-A

◂ **Fig. 5** ADAM17 activation or deletion of JAM-A/F11R impairs WSS-dependent endothelial cell alignment. Endothelial cell orientation was quantified in vitro in order to assess WSS response as indicated by cell alignment relative to flow direction. HUVECs were transfected with scrambled (Control) siRNA, exposed to recombinant ADAM17 protein, or transfected with JAM-A/F11R siRNA. HUVECs were then subjected to WSS (8 dyne/cm^2 flow, for 72 h) and orientation distribution frequency percentage relative to flow direction was measured using the ImageJ directionality plugin or angle measurement tool. Cell frequency in different orientation distribution (**a**–**c**), cell average orientation degree (**d**), and representative images (**e**, **f**) obtained from 4 independent experiments are shown at 0, 24, 48, and 72 h of culture. Data on panel d are presented as box-and-whisker plots, in which the minimum, the 25th percentile, the median, the 75th percentile, and the maximum are shown, + indicates the mean of values. For statistical analyses, ordinary two-way ANOVA with Sidak's multiple comparison test was used. *$p < 0.05$ compared to control siRNA

assess the role of WSS in their experiments, so the primary physical stimulus to initiate endothelial NO production remains unknown. Interestingly, in their study, Sun and his colleagues found that a reduced flow-induced dilation is caused by impaired WSS sensitivity in skeletal muscle resistance arteries of adult rats [46]. Our present experiments, using isolated skeletal muscle resistance arteries of aged mice, revealed that WSS-induced vasodilation was not only reduced in magnitude, but required a significantly greater WSS level (~25 vs. 10 dyne/cm^2, aged vs. young respectively) to reach the maximum vasodilator response. At any given flow rate, the calculated WSS was found to be much higher in aged mice, when compared to the arteries of young animals. Along with these changes, we observed that the overall blood flow velocity in the femoral artery remains unchanged in the aged mice. Therefore, our results imply a significant reduction in the ability of endothelium in aged resistance arteries to sense the biomechanical force, WSS. Our present results challenge the current views and indicate a selective impairment of WSS mechanosensing by the vascular endothelium in aging, which in turn fails to initiate signaling mechanisms, including WSS-induced production of NO. This could lead to a diminished antiproliferative effect on vascular smooth muscle cells, thereby promoting hypertrophic remodeling of the resistance arteries in aged mice.

In this study, we also examined the mechanisms that are responsible for age-related impairment of endothelial WSS mechanosensing. Previously, we reported that adipose tissue resistance arteries of elderly human subjects and aged mice display a significant upregulation of vascular endothelial ADAM17, which is associated with TNF-mediated remote coronary artery dysfunction [13]. ADAM17-dependent transactivation of epidermal growth factor receptor has been previously implicated in the development of vascular wall hypertrophy which is induced by angiotensin II [35, 47]. Because in our current study we found an almost four-fold upregulation of ADAM17 in the skeletal muscle arteries of aged mice, we postulated a key mechanistic role of ADAM17 in the development of impaired WSS sensing and abnormal vascular remodeling. ADAM17 is a crucial regulator of many physiological and pathological functions, including inflammatory processes and vascular development [20]. ADAM17 exerts its effects by proteolytic shedding of various cell membrane-bound molecules, such as TNF, epidermal growth factor, transforming growth factor α, and JAM-A/F11R, among others [19]. The proteolytic cleavage of the ADAM17-targeted molecule could result in activation of cellular signaling pathways [19] or alterations in the subcellular distribution of the substrate [27, 39]. In this latter context, Koenen et al. reported that ADAM17-mediated cleavage of JAM-A/F11R leads to a redistribution of JAM-A/F11R from cellular junctions to the apical surface, thereby making JAM-A/F11R accessible to support the adhesion of leukocytes [27]. Because earlier it was found that JAM-A/F11R can also act as a mechanosensor [41, 49], we raised the possibility that ADAM17 activation interferes with WSS mechanosensing through a process that involves ADAM17-mediated cleavage of JAM-A/F11R. To test this possibility, first we determined the protein expression and subcellular distribution of JAM-A/F11R using Western immunoblotting and *en face* immunostaining of the aorta from young and aged mice, as well as employed endothelial cells with ADAM17 activation cultured under steady WSS condition. We observed that without changes in the overall expression, the endothelial cell junction-localized JAM-A/F11R was significantly reduced in aged mice and also in cultured endothelial cells with ADAM17

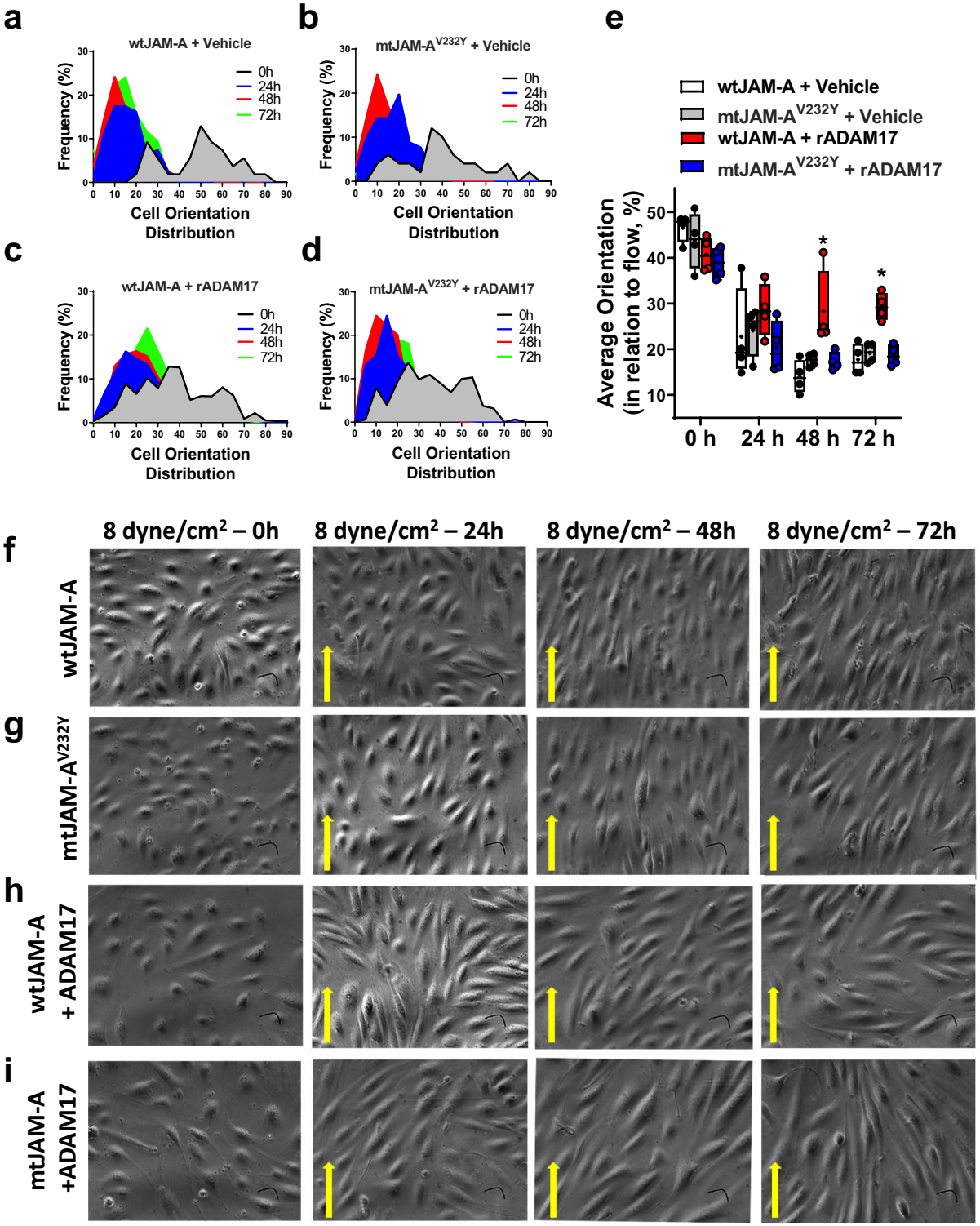
a
wtJAM-A + Vehicle
Frequency (%)
0h
24h
48h
72h
Cell Orientation Distribution
b
mtJAM-A^{V232Y} + Vehicle
c
wtJAM-A + rADAM17
d
mtJAM-A^{V232Y} + rADAM17
e
wtJAM-A + Vehicle
mtJAM-A^{V232Y} + Vehicle
wtJAM-A + rADAM17
mtJAM-A^{V232Y} + rADAM17
Average Orientation (in relation to flow, %)
0 h
24 h
48 h
72 h
f
8 dyne/cm^2 – 0h
8 dyne/cm^2 – 24h
8 dyne/cm^2 – 48h
8 dyne/cm^2 – 72h
wtJAM-A
g
mtJAM-A^{V232Y}
h
wtJAM-A + ADAM17
i
mtJAM-A +ADAM17

◂ **Fig. 6** Endothelial cells expressing the ADAM17 cleavage resistant JAM-A/F11R sufficiently align to flow direction. HUVECs were transfected with wild type human JAM-A/F11R (wtJAM-A) or ADAM17 cleavage resistant mutant human JAM-A/F11R (mtJAM-A^{V232Y}) plasmids and subsequently were exposed to recombinant ADAM17 protein or vehicle. HUVECs were subjected to WSS (8 dyne/cm^2 flow, for 72 h) and orientation distribution frequency percentage (**a**–**d**) relative to flow direction was measured using the ImageJ directionality plugin or angle measurement tool. The average orientation degree (**e**) and representative images (**f**–**i**) from 4 independent experiments are shown at 0, 24, 48, and 72 h of culture. Data on panel e are presented as box-and-whisker plots, in which the minimum, the 25th percentile, the median, the 75th percentile, and the maximum are shown, + indicates the mean of values. For statistical analyses, ordinary two-way ANOVA with Sidak's multiple comparison test was used. $*p < 0.05$ compared to wtJAM-A + vehicle group

activation. We also found that JAM-A/F11R depleted endothelial cells cultured under steady WSS conditions were elongated but failed to align in the direction of flow. Thus, unveiling a novel role for JAM-A/F11R in the endothelial WSS mechanosensory process, particularly in sensing flow direction. In addition, after overexpression of ADAM17 cleavage resistant JAM-A/F11R (mtJAM-A^{V232Y}), we found that endothelial cells were efficiently elongated and aligned to the direction of flow, even after ADAM17 activation. These results underscore a specific defect in sensing WSS and flow direction after ADAM17 activation, which is likely to be mediated by the excess cleavage and redistribution of the endothelial cell junction-localized JAM-A/F11R.

Because results obtained in the mouse aorta cannot be directly extrapolated to resistance arteries, and due to limitations inherent of cultured endothelial cells, the role of upregulated ADAM17 and JAM-A/F11R in contributing to aging-related impairment of WSS sensing and abnormal arterial remodeling experiments were also performed in vivo. To that end, a confined, unilateral intra-arteriolar delivery of AAV encoding mouse ADAM17 or the ADAM17 cleavage resistant mutant mouse JAM-A/F11R (mtJAM-A^{V232Y}) was utilized in young or aged mice, respectively. Two weeks after the AAV-mediated overexpression of ADAM17, the targeted skeletal muscle resistance artery segment, but not the contralateral control, of young mice displayed a reduced WSS-induced vasodilation, which was accompanied by vascular wall hypertrophy and increased wall to lumen ratio. Neither agonist-induced vasodilation nor the luminal diameter, measured at different intraluminal pressure levels, was changed significantly by the focal delivery of mouse ADAM17. These results obtained in young mice recapitulate the aged vascular phenotype that ADAM17 induces a selective impairment of WSS mechanosensing and elicits a hypertrophic arterial remodeling. Using a similar, AAV-mediated gene delivery approach, the ADAM17 cleavage-resistant mutant mouse JAM-A/F11R (mtJAM-A^{V232Y}) was focally overexpressed in the skeletal muscle resistance artery segment of the aged mice. Notable, 2 weeks after delivery of the ADAM17 cleavage-resistant mouse JAM-A/F11R, the impaired WSS-induced vasodilator response was reversed and normalized in the aged mice when compared to contralateral artery segment. We observed no reversal effects on vascular wall hypertrophy and luminal dimension and found no changes in vasodilation in response to agonists in skeletal muscle resistance artery segments expressing the cleavage-resistant mtJAM-A^{V232Y}. Results from these rescue experiments obtained in the aged mice signify the role of ADAM17 in excess cleavage of JAM-A/F11R in the aged arteriolar wall leading to impaired WSS mechanosensing. The inability to reverse age-related vascular hypertrophy can be interpreted that although there might be more NO production and inhibition of vascular smooth muscle proliferation, it might need a longer time to achieve significant effects compare to the contralateral arteries. The other way to interpret is ADAM17-dependent mechanisms other than JAM-A/F11R cleavage, such as mediated by epidermal growth factor receptor transactivation [35, 47] may also play a role in this process, a scenario that has yet to be examined in future studies.

Vascular remodeling is uniquely driven by mechanical forces from blood flow in which WSS mechanosensing by the endothelial cells plays a pivotal role [1, 2]. Schwartz and his colleagues recently proposed a concept in which the vascular endothelium encodes a WSS set point, which governs vascular remodeling and has major implications in vascular development and vascular graft adaptation, among others [3]. In the present study, we describe a novel mechanism, by which the ADAM17-mediated

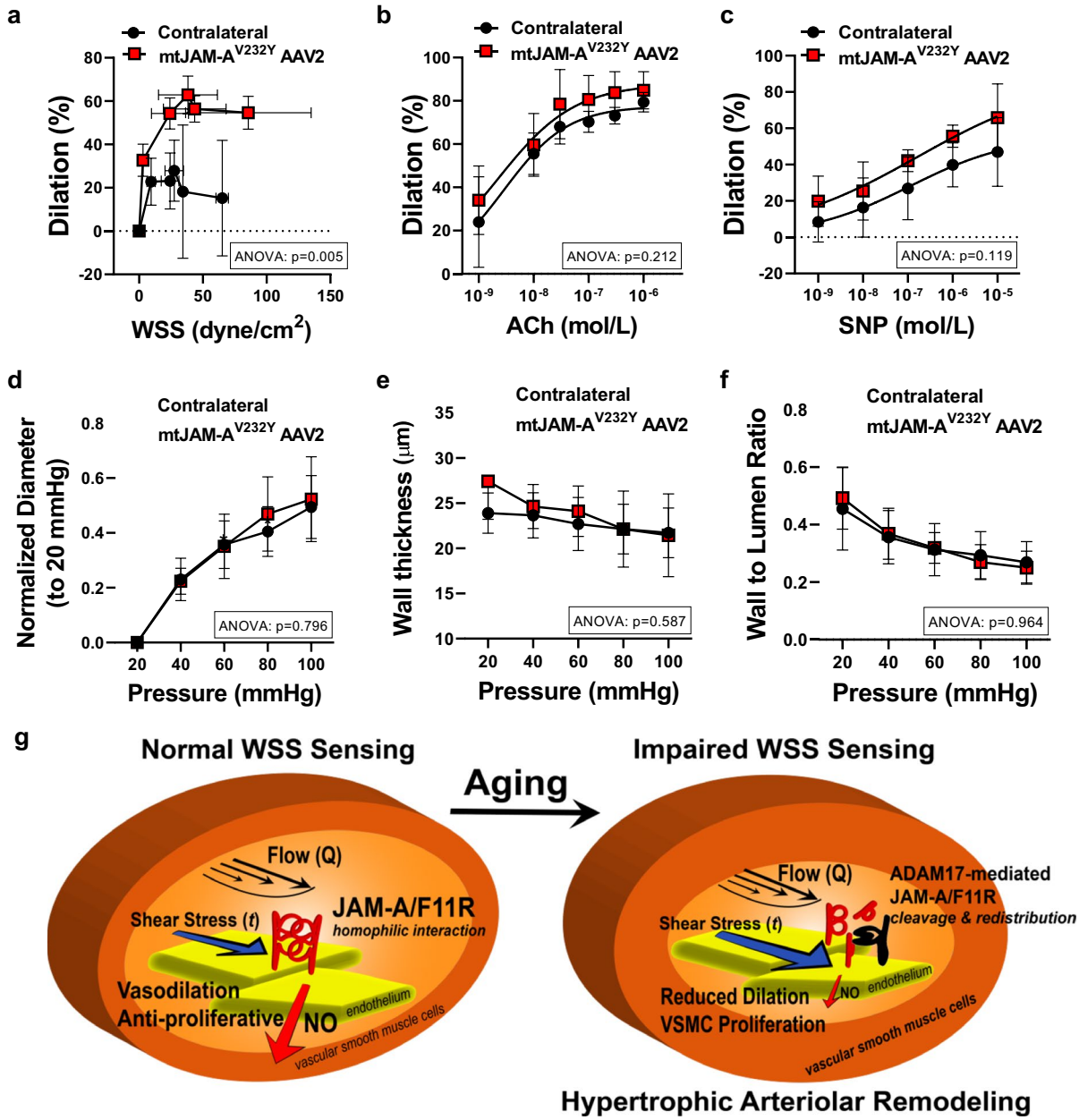

reduced mechanosensing of WSS, rather than the magnitude of flow, and therefore, the absence of WSS-initiated signaling mechanisms (e.g., diminishing release of vasodilator and antiproliferative NO) determines hypertrophic, lumen narrowing remodeling of small resistance arteries in aging (Fig. 7g). Based on our results, we propose that an augmented ADAM17-mediated cleavage and redistribution of JAM-A/F11R underlie the aging-related impairment of WSS sensing mechanisms, which results in an abnormal, lumen narrowing vascular remodeling in aging. Conceptually, ADAM17 could prove to be a direct, novel regulator of WSS mechanosensing, whereby it can play a crucial role in the control of both normal vascular growth and pathological vascular remodeling.

◂ **Fig. 7** Focal overexpression of ADAM17 cleavage resistant mouse JAM-A^{V232Y} augments WSS-induced vasodilation in aged mice. Summary data ($n=3$, in each group) of percent diameter changes of isolated left ipsilateral (mutant mouse JAM-A^{V232Y} AAV2QuadYF injected) and right (contralateral) skeletal (m. gracilis) arteries in response to increased WSS (**a**) or cumulative concentrations of acetylcholine (ACh, 10^{-9} to 10^{-6} mol/L) (**b**) and NO donor, sodium nitroprusside (SNP, 10^{-9} to 10^{-5} mol/L) (**c**). Summary data ($n=3$, in each group) of inner normalized diameter (to initial diameter at 20 mmHg) (**d**), wall thickness (**e**), and wall-to-lumen ratio (**f**) in relation to increases in intraluminal pressure from 20 to 100 mmHg in isolated left ipsilateral (mtJAM-A^{V232Y} AAV-2QuadYF injected) and right (contralateral) skeletal (m. gracilis) arteries. Data are mean ± SEM. For data analyses repeated measures two-way ANOVA (ANOVA p value for the corresponding effects are shown in the insets) with Sidak multiple comparisons were used (contralateral vs. ipsilateral artery). (**g**) Schematic drawing illustrates the proposed novel mechanism in which reduced mechanosensing of WSS (t), rather than the magnitude of flow (Q), determines reduced vasodilation and abnormal remodeling of small resistance arteries in aging. In young mice (left) small resistance arteries with normal WSS sensing, JAM-A/F11R participates in WSS mechanosensing and NO production to induce vasodilation and to exert an anti-proliferative effect on the vascular smooth muscle cells. In arteries of aged mice (right) an augmented ADAM17-mediated cleavage and redistribution of JAM-A/F11R underlies impaired WSS sensing, which leads to a reduced vasodilation and promotes vascular smooth muscle cells proliferation, thereby causing an inward hypertrophic arterial remodeling, independent of blood flow velocity and even in the presence of increased WSS levels

Author contribution Z.B. conceptualized the project. Z.B., Y.T., H.D., K.A.F., L.L., and V.B. performed the experiments. Y.T and Z.B wrote the original draft of the manuscript. Y.T., H.D., K.A.F., V.B., L.L., R.D.R., J.A.F, and Z.B. reviewed and edited the manuscript. Z.B. supervised the research.

Funding This work was supported by awards from the American Heart Association [20PRE35211126 to YT] and National Institutes of Health, National Institute on Aging [R01AG054651 to ZB].

Data availability We declare that the data supporting the findings of this study are available within the article and its Supplementary Information files and from the corresponding authors upon request.

Declarations

Conflict of interest The authors declare no conflict of interest.

References

1. Baeyens N, Bandyopadhyay C, Coon BG, Yun S, Schwartz MA. Endothelial fluid shear stress sensing in vascular health and disease. J Clin Invest. 2016;126:821–8.
2. Baeyens N, Larrivee B, Ola R, Hayward-Piatkowskyi B, Dubrac A, Huang B, Ross TD, Coon BG, Min E, Tsarfati M, Tong H, Eichmann A, Schwartz MA. Defective fluid shear stress mechanotransduction mediates hereditary hemorrhagic telangiectasia. J Cell Biol. 2016;214:807–16.
3. Baeyens N, Nicoli S, Coon BG, Ross TD, Van den Dries K, Han J, Lauridsen HM, Mejean CO, Eichmann A, Thomas JL, Humphrey JD, Schwartz MA. Vascular remodeling is governed by a VEGFR3-dependent fluid shear stress set point. Elife. 2015;4:e04645.
4. Bagi Z, Koller A. Lack of NO-mediation of flow-dependent arteriolar dilation in diabetes is restored by sepiapterin. J of Vascular Research. 2003;40:47–57.
5. Bagi Z, Frangos JA, Yeh JC, White CR, Kaley G, Koller A. PECAM-1 mediates NO-dependent dilation of arterioles to high temporal gradients of shear stress. Arterioscler Thromb Vasc Biol. 2005;25:1590–5.
6. Bearden SE, Payne GW, Chisty A, Segal SS. Arteriolar network architecture and vasomotor function with ageing in mouse gluteus maximus muscle. J Physiol. 2004;561:535–45.
7. Beyer AM, Zinkevich N, Miller B, Liu Y, Wittenburg AL, Mitchell M, Galdieri R, Sorokin A, Gutterman DD. Transition in the mechanism of flow-mediated dilation with aging and development of coronary artery disease. Basic Res Cardiol. 2017;112:5.
8. Buus CL, Pourageaud F, Fazzi GE, Janssen G, Mulvany MJ, De Mey JG. Smooth muscle cell changes during flow-related remodeling of rat mesenteric resistance arteries. Circ Res. 2001;89:180–6.
9. Csiszar A, Ungvari Z, Edwards JG, Kaminski P, Wolin MS, Koller A, Kaley G. Aging-induced phenotypic changes and oxidative stress impair coronary arteriolar function. Circ Res. 2002;90:1159–66.
10. Dao HH, Essalihi R, Bouvet C, Moreau P. Evolution and modulation of age-related medial elastocalcinosis: impact on large artery stiffness and isolated systolic hypertension. Cardiovasc Res. 2005;66:307–17.
11. Davies PF. Flow-mediated endothelial mechanotransduction. Physiol Rev. 1995;75:519–60.
12. Donato AJ, Machin DR, Lesniewski LA. Mechanisms of dysfunction in the aging vasculature and role in age-related disease. Circ Res. 2018;123:825–48.
13. Dou H, Feher A, Davila AC, Romero MJ, Patel VS, Kamath VM, Gooz MB, Rudic RD, Lucas R, Fulton DJ, Weintraub NL, Bagi Z. Role of adipose tissue endothelial ADAM17 in age-related coronary microvascular dysfunction. Arterioscler Thromb Vasc Biol. 2017;37:1180–93.
14. Ebnet K. Junctional adhesion molecules (JAMs): cell adhesion receptors with pleiotropic functions in cell physiology and development. Physiol Rev. 2017;97:1529–54.

15. Ebnet K, Suzuki A, Ohno S, Vestweber D. Junctional adhesion molecules (JAMs): more molecules with dual functions? J Cell Sci. 2004;117:19–29.
16. Erdei N, Toth A, Pasztor ET, Papp Z, Edes I, Koller A, Bagi Z. High-fat diet-induced reduction in nitric oxide-dependent arteriolar dilation in rats: role of xanthine oxidase-derived superoxide anion. Am J Physiol Heart Circ Physiol. 2006;291:H2107–15.
17. Garton KJ, Gough PJ, Philalay J, Wille PT, Blobel CP, Whitehead RH, Dempsey PJ, Raines EW. Stimulated shedding of vascular cell adhesion molecule 1 (VCAM-1) is mediated by tumor necrosis factor-alpha-converting enzyme (ADAM 17). J Biol Chem. 2003;278:37459–64.
18. Gerhard M, Roddy MA, Creager SJ, Creager MA. Aging progressively impairs endothelium-dependent vasodilation in forearm resistance vessels of humans. Hypertension. 1996;27:849–53.
19. Gooz M. ADAM-17: the enzyme that does it all. Crit Rev Biochem Mol Biol. 2010;45:146–69.
20. Gooz P, Gooz M, Baldys A, Hoffman S. ADAM-17 regulates endothelial cell morphology, proliferation, and in vitro angiogenesis. Biochem Biophys Res Commun. 2009;380:33–8.
21. Hajdu MA, Heistad DD, Siems JE, Baumbach GL. Effects of aging on mechanics and composition of cerebral arterioles in rats. Circ Res. 1990;66:1747–54.
22. Hall JE, Brands MW, Henegar JR. Mechanisms of hypertension and kidney disease in obesity. Ann N Y Acad Sci. 1999;892:91–107.
23. Heiss, C., R. Sansone, H. Karimi, M. Krabbe, D. Schuler, A. Rodriguez-Mateos, T. Kraemer, M. M. Cortese-Krott, G. G. Kuhnle, J. P. Spencer, H. Schroeter, M. W. Merx, M. Kelm, and European Union th Framework Program Flaviola Consortium. Impact of cocoa flavanol intake on age-dependent vascular stiffness in healthy men: a randomized, controlled, double-masked trial. Age (Dordr). 2015;37:9794.
24. Jackson DN, Moore AW, Segal SS. Blunting of rapid onset vasodilatation and blood flow restriction in arterioles of exercising skeletal muscle with ageing in male mice. J Physiol. 2010;588:2269–82.
25. Kenwright DA, Thomson AJ, Hadoke PW, Anderson T, Moran CM, Gray GA, Hoskins PR. A protocol for improved measurement of arterial flow rate in preclinical ultrasound. Ultrasound Int Open. 2015;1:E46-52.
26. Ko KA, Fujiwara K, Krishnan S, Abe JI. En Face preparation of mouse blood vessels. J Vis Exp. 2017;123:e55460.
27. Koenen RR, Pruessmeyer J, Soehnlein O, Fraemohs L, Zernecke A, Schwarz N, Reiss K, Sarabi A, Lindbom L, Hackeng TM, Weber C, Ludwig A. Regulated release and functional modulation of junctional adhesion molecule A by disintegrin metalloproteinases. Blood. 2009;113:4799–809.
28. Koller A, Kaley G. Endothelium regulates skeletal muscle microcirculation by a blood flow velocity-sensing mechanism. Am J Physiol. 1990;258:H916–20.
29. Koller A, Kaley G. Endothelial regulation of wall shear stress and blood flow in skeletal muscle microcirculation. Am J Physiol. 1991;260:H862–8.
30. Laurant P, Adrian M, Berthelot A. Effect of age on mechanical properties of rat mesenteric small arteries. Can J Physiol Pharmacol. 2004;82:269–75.
31. Martinez-Lemus LA, Hill MA, Meininger GA. The plastic nature of the vascular wall: a continuum of remodeling events contributing to control of arteriolar diameter and structure. Physiology (Bethesda). 2009;24:45–57.
32. Meschiari CA, Ero OK, Pan H, Finkel T, Lindsey ML. The impact of aging on cardiac extracellular matrix. Geroscience. 2017;39:7–18.
33. Mulvany MJ. Vascular remodelling of resistance vessels: can we define this? Cardiovasc Res. 1999;41:9–13.
34. Ohanian J, Liao A, Forman SP, Ohanian V. Age-related remodeling of small arteries is accompanied by increased sphingomyelinase activity and accumulation of long-chain ceramides. Physiol Rep. 2014;2:e12015.
35. Ohtsu H, Dempsey PJ, Frank GD, Brailoiu E, Higuchi S, Suzuki H, Nakashima H, Eguchi K, Eguchi S. ADAM17 mediates epidermal growth factor receptor transactivation and vascular smooth muscle cell hypertrophy induced by angiotensin II. Arterioscler Thromb Vasc Biol. 2006;26:e133–7.
36. Paneni F, Diaz Canestro C, Libby P, Luscher TF, Camici GG. The aging cardiovascular system: understanding it at the cellular and clinical levels. J Am Coll Cardiol. 2017;69:1952–67.
37. Pistea A, Bakker EN, Spaan JA, VanBavel E. Flow inhibits inward remodeling in cannulated porcine small coronary arteries. Am J Physiol Heart Circ Physiol. 2005;289:H2632–40.
38. Pourageaud F, De Mey JG. Structural properties of rat mesenteric small arteries after 4-wk exposure to elevated or reduced blood flow. Am J Physiol. 1997;273:H1699–706.
39. Pruessmeyer J, Martin C, Hess FM, Schwarz N, Schmidt S, Kogel T, Hoettecke N, Schmidt B, Sechi A, Uhlig S, Ludwig A. A disintegrin and metalloproteinase 17 (ADAM17) mediates inflammation-induced shedding of syndecan-1 and -4 by lung epithelial cells. J Biol Chem. 2010;285:555–64.
40. Schaper W. Collateral circulation: past and present. Basic Res Cardiol. 2009;104:5–21.
41. Scott DW, Tolbert CE, Burridge K. Tension on JAM-A activates RhoA via GEF-H1 and p115 RhoGEF. Mol Biol Cell. 2016;27:1420–30.
42. Shipley RD, Muller-Delp JM. Aging decreases vasoconstrictor responses of coronary resistance arterioles through endothelium-dependent mechanisms. Cardiovasc Res. 2005;66:374–83.
43. Silvestre JS, Levy BI, Tedgui A. Mechanisms of angiogenesis and remodelling of the microvasculature. Cardiovasc Res. 2008;78:201–2.
44. Silvestre JS, Smadja DM, Levy BI. Postischemic revascularization: from cellular and molecular mechanisms to clinical applications. Physiol Rev. 2013;93:1743–802.
45. Solimando AG, Brandl A, Mattenheimer K, Graf C, Ritz M, Ruckdeschel A, Stuhmer T, Mokhtari Z, Rudelius M, Dotterweich J, Bittrich M, Desantis V, Ebert R, Trerotoli P, Frassanito MA, Rosenwald A, Vacca A, Einsele H, Jakob F, Beilhack A. JAM-A as a prognostic factor and new therapeutic target in multiple myeloma. Leukemia. 2018;32:736–43.
46. Sun D, Huang A, Koller A, Kaley G. Decreased arteriolar sensitivity to shear stress in adult rats is reversed by chronic exercise activity. Microcirculation. 2002;9:91–7.

47. Takayanagi T, Forrester SJ, Kawai T, Obama T, Tsuji T, Elliott KJ, Nuti E, Rossello A, Kwok HF, Scalia R, Rizzo V, Eguchi S. Vascular ADAM17 as a novel therapeutic target in mediating cardiovascular hypertrophy and perivascular fibrosis induced by angiotensin II. Hypertension. 2016;68:949–55.
48. Tkachenko E, Gutierrez E, Saikin SK, Fogelstrand P, Kim C, Groisman A, Ginsberg MH. The nucleus of endothelial cell as a sensor of blood flow direction. Biol Open. 2013;2:1007–12.
49. Tornavaca O, Chia M, Dufton N, Almagro LO, Conway DE, Randi AM, Schwartz MA, Matter K, Balda MS. ZO-1 controls endothelial adherens junctions, cell-cell tension, angiogenesis, and barrier formation. J Cell Biol. 2015;208:821–38.
50. Tran L, Greenwood-Van Meerveld B. Age-associated remodeling of the intestinal epithelial barrier. J Gerontol A Biol Sci Med Sci. 2013;68:1045–56.
51. Tsakadze NL, Sithu SD, Sen U, English WR, Murphy G, D'Souza SE. Tumor necrosis factor-alpha-converting enzyme (TACE/ADAM-17) mediates the ectodomain cleavage of intercellular adhesion molecule-1 (ICAM-1). J Biol Chem. 2006;281:3157–64.
52. Tzima E, Irani-Tehrani M, Kiosses WB, Dejana E, Schultz DA, Engelhardt B, Cao G, DeLisser H, Schwartz MA. A mechanosensory complex that mediates the endothelial cell response to fluid shear stress. Nature. 2005;437:426–31.
53. Ungvari Z, Tarantini S, Donato AJ, Galvan V, Csiszar A. Mechanisms of vascular aging. Circ Res. 2018;123:849–67.
54. Ungvari Z, Tarantini S, Nyul-Toth A, Kiss T, Yabluchanskiy A, Csipo T, Balasubramanian P, Lipecz A, Benyo Z, Csiszar A. Nrf2 dysfunction and impaired cellular resilience to oxidative stressors in the aged vasculature: from increased cellular senescence to the pathogenesis of age-related vascular diseases. Geroscience. 2019;41:727–38.
55. Wawro K, Wawro M, Strzelecka M, Czarnek M, Bereta J. The role of NF-kappaB and Elk-1 in the regulation of mouse ADAM17 expression. Biol Open. 2019;8:bio039420.
56. Wu L, Claas AM, Sarkar A, Lauffenburger DA, Han J. High-throughput protease activity cytometry reveals dose-dependent heterogeneity in PMA-mediated ADAM17 activation. Integr Biol (Camb). 2015;7:513–24.
57. Xu H, Lu S, Ding L, Lyu L, Ma Z, Lu Q. Pulsatility index as a novel parameter for perfusion in mouse model of hindlimb ischemia. Cell Physiol Biochem. 2018;48:2114–22.
58. Zhou J, Li YS, Chien S. Shear stress-initiated signaling and its regulation of endothelial function. Arterioscler Thromb Vasc Biol. 2014;34:2191–8.